Optimized Isolation and Characterization of Cellulose for Extraction of Cellulose Nanocrystals from Ensete Ventricosum Pseudo-Stem Fiber Using Two-Stage Extraction Method

Abnet Mengesha Dube (abnetm817@gmail.com)
Wolkite University
Bulcha Jifara Daba
Haromaya University Institute of Technology, Haromaya University
Melkiyas Diriba Muleta
Haromaya University Institute of Technology, Haromaya University

Research Article

Keywords: Alkali treatment, Delignification, Ensete ventricosum pseudo stem fiber, Cellulose, Response surface methodology, Reaction parameters

Posted Date: October 19th, 2022

DOI: https://doi.org/10.21203/rs.3.rs-2151793/v1

Abstract

Alkali treatment followed by alkalinized hydrogen peroxide delignification yielded 73.90% cellulose from *Ensete Ventricosum* pseudo stem fiber, with parameters optimized using response surface methodology. The optimal reaction parameters were 157 minutes, 73 ℃, and 3.8% NaOH concentration. Thermogravimetric analysis (TGA), X-ray diffraction (XRD), Fourier transfer infrared (FTIR), and scanning electron microscopy were used to examine the thermal properties, crystal structure, chemical structure, and morphological structure of isolated cellulose (SEM). Based on the findings, cellulose has a rod-like shape. The XRD results revealed that the crystallinity index of cellulose increased from 65 to 75 percent when compared with raw Ensete*ventricosum* pseudo stem fiber (Ensete fiber). The resultant cellulose demonstrated relatively higher thermal stability than the unprocessed ensete fiber, according to the thermogravimetric examination. When compared to raw ensete fiber, FTIR analysis revealed that cellulose had a modified chemical functional structure, which suggested that alkali and alkalized hydrogen peroxide treatments had altered the chemical structure of cellulose. According to the results, it is possible to extract cellulose nanocrystals thanks to the isolated cellulose's high yield, great crystallinity index, strong thermal stability, and morphological structure.

Highlights

- Two step pretreatment was employed to extract cellulose from ensete fiber.
- Isolated cellulose characterized for it morphological, thermal, functional changes.
- Cellulose from ensete fiber exhibited good thermal, physical, chemical properties.
- X-ray diffractometer result depicted that cellulose from ensete fiber has good crystallinity.
- Cellulose extraction condition was optimized to obtain optimum yield of cellulose.

Introduction

The development of environmentally friendly materials has attracted a lot of attention due to the depletion of petroleum-based resources and a number of environmental difficulties, including health problems and global warming (Miao et al., 2014). To solve environmental issues, bio-based materials such as biomass waste, agricultural byproducts, forestry waste, natural fibers, and so on, could be employed as viable substitutes for petroleum-based materials (Abdul Khalil et al., 2007). These materials have benefits, including low cost, abundance, biodegradability, renewability, and environmental friendliness (Flauzino Neto et al., 2013; Henrique et al., 2013). One of these bio-based materials that potentially takes the place of petroleum-based components is biomass from the *Ensete ventricosum* plant.

Ensete ventricosum (Enset (Welw.) Cheesman) is a native herbaceous crop with many uses. It is mostly grown in Ethiopia's Southern, Sidama, South Western, and Oromia regions (Cheesman et al., 2022). It is a food crop that is only grown in Ethiopia, and little is known about it (Zerihun Yemataw, Henoke Fikre, Sadik Muzemil, 2021). Bulla, Kocho, and Amicho are three foods made from the crop that are excellent sources of starch and carbohydrates (Olango et al., 2014a; Yemataw et al., 2018). Additionally, this plant is an excellent source of fiber and animal feed (Seid et al., 2022). *Enset* can be grown in a much larger area to feed more than 100 million people and improve food security in Ethiopia, Kenya, Uganda, and Rwanda, according to recent modeling studies. The plant's capacity to be cultivated and harvested at any time of the year demonstrates its adaptability to changing climates (Zerihun Yemataw, Henoke Fikre, Sadik Muzemil, 2021).

The plant is widely grown in the nation as food for a big population, and as a result of the extensive food production process and cultivation, enormous amounts of waste lignocellulose biomass are sourced (Dube, 2022; Nurfeta, Eik, et al., 2008; Yemata, 2020). The plant's leaves, pseudo-stem (a bundle of fibers), and main stalk of *ensete ventricosum* are the main sources of these residual wastes (Berhanu et al., 2018; Fekadu & Ledin, 1997; Tsegaye & Struik, 2021). According to various studies, the leaf lamina, leaf midribs, pseudo stem, and corm are the four fractional portions that make up the majority of *ensete ventricosum's* dry matter (Fig. 1) (Nurfeta, Eik, et al., 2008). These four dry matter fractions have different compositions depending on the kind, region, season, etc. of the plant (Bosha et al., 2019; Olango et al., 2014b; Yemata, 2020). Different *Ensete ventricosum* types have different ratios of these four ingredients. Leaf lamina is 6–17 percent, the pseudo stem is 45–60 percent, stalk is 4–21 percent, and corm is 10–30 percent, according to research findings (Fekadu & Ledin, 1997; Mohammed et al., 2013; Nurfeta, Eik, et al., 2008; Nurfeta, Tolera, et al., 2008). The pseudo stem fraction is larger than the other fractional sections, as shown in these reports, and it is primarily made up of pulpy parts, long and thin fibers with low extractive, ash, and lignin content (4.4, 3.8, and 10.5 percent, respectively). The pseudo stem fiber (one of the musa plant's fibers) has a high holocellulose and cellulose content (87.5 and 59.5 percent, respectively) (Berhanu et al., 2018; Dube, 2022; Gabriel et al., 2020). Unfortunately, Ethiopia's resources for *ensete ventricosum* pseudo stem natural fiber have not been used to their full potential. This natural fiber is mostly made up of two polysaccharides cellulose, hemicellulose, and one aromatic polymer lignin as well as small amounts of moisture, ash, and extractives (Fekadu & Ledin, 1997; Teli & Terega, 2017). According to its chemical makeup, cellulose is the main polysaccharide of *ensete ventricosum's* pseudo-stem fiber.

Therefore, there is significant potential in isolating cellulose from *ensete ventricosum* pseudo stem fiber for many applications, including cellulose nanocrystals, polymers, textiles, and so forth. Cellulose is the most important natural product created by living organisms because it forms the structural basis of the cell wall of lignocellulose biomass (ASPINALL, 1980). This polymer, which is essential for preserving the structure of plant cell walls, often comprises of fibrous, water-insoluble, rigid crystalline substance (Habibi et al., 2010). It is one of the major natural polymers in lignocellulose biomass, which is composed of linear β-1, 4 glycosidic chains of glucose molecules that make it a rigid and insoluble crystalline polymer (Davison et al., 2013; Gong et al., 2017). Cellulose is made up of microfibrils, which are collections of fibrils. However, each individual fibril has both crystalline and amorphous domains (Mtibe et al., 2015). For use in various application areas, non-cellulose components of fibers can be broken down using chemical or mechanical processes to produce cellulose (Lin et al., 2021).

Cellulose extraction can be seen as one of several effective pretreatment techniques for the elimination of undesirable components in the development of various products from cellulose in various application areas (Southon & Magana, 2010). To be used in a variety of fields, including biomedical, adsorbents, nanocomposite, energy, food, and packaging materials, Nano cellulose required some extraordinary properties, including a unique nanostructure, hydrophilicity, low toxicity, biocompatibility, biodegradability, ease of modification, and high mechanical properties (Dufresne, 2019; Klemm et al., 2018; Owolabi et al., 2020). Various mechanical, chemical, or chemo-mechanical extraction techniques have been published in the past few years to extract cellulose from lignocellulose biomasses (Rojas, 2016; Xing et al., 2018). Different techniques, including hydrothermal extraction, conventional alkali extraction, ambient condition extraction, and two-stage extraction, can be used to extract cellulose (Lin et al., 2021). One of the most popular methods for biomass to isolate cellulose from and enhance the mechanical and thermal stability of the extracted cellulose for cellulose nanocrystals is alkali solution treatment (Zhang et al., 2015). This study use the two stage alkali and hydrogen peroxide delignification extraction process to get enhanced morphology, dimension, chemical composition, hydrogen bonding system, and other properties.

A thorough investigation is needed to develop the use of *ensete ventricosum* pseudo stem fiber, improve its economic potential, and ensure its sustainability. Even though this subject has been the subject of research, it is still vital to examine its potential from those angles in order to make the most of it. The renewability, abundancy, low cost, underutilization, and biodegradability of this natural fiber are of the intriguing qualities that have made it a candidate for usage in military vehicles, textiles, biomedical applications, structural and building construction, automotive, aerospace, and other industries. The goal of this study was to extract cellulose from *ensete ventricosum* pseudo stem natural fiber so that it could be used to isolate cellulose nanocrystals.

Material And Methods

Materials

Ensete ventricosum pseudo stem fiber was purchased and collected from local farms (Gurage Zone, Ethiopia). Chloroform (99%), hydrogen peroxide (30%), and acetic acid (99.5%), sodium hypochlorite, toluene (99%), ethanol (97%), sulfuric acid (97%), sodium hydroxide (97%) were purchased from Fine chemical PLC (Addis Ababa, Ethiopia). All used chemicals were of analytical grade and double distilled water was used in the study.

Preparation of Cellulose

Mechanical treatments and oxidation reaction of the fiber were similar with the one performed in previous research by the same researcher (Dube, 2022). The removal of great amount of hemicellulose was achieved by alkali treatment. Mechanically treated ground and wax free ensete fiber was treated with solution of sodium hydroxide. The alkali treatment process performed at different reaction condition (sodium hydroxide concentration: 2–5%; reaction time: 120–240 min and temperature: 50–100 ℃) and fixed cellulose to sodium hydroxide ratio 1:20 (w/v). Continuous mechanical mixing was employed with speed of 750 rpm. By introducing cold water (4 ℃) into the reaction beaker the process was stopped. Double distilled water used to remove stacked sodium hydroxide to surface of solid cake. The process was continued until neutral pH was obtained. Then the solid cake was dried for 24 hours at 45 ℃ for the next process (Dube, 2022).

Calculation of Cellulose Yield

Raw ensete fiber and alkali treated fiber were studied for their chemical compositions (cellulose, hemicellulose, and lignin). The alkali treated fiber cellulose content was studied at each reaction points and at final optimized point. All the experiments were performed three times according to standards, protocols and previous works(Dube, 2022).

Experimental Design

An empirical modeling method used in the creation of experimental models and experiment design using response surface methodology (RSM). The surface plotting and statistical analysis were done with Design-Expert 11. The three independent variables were sodium hydroxide concentration (2, 3.5, and 5%), reaction time (120, 180, and 240 min), and reaction temperature (50, 75, and 100°C). The yield of cellulose was the outcome, and the selection range for each variable was displayed in Table 1.

Table 1
Response to cellulose yield and the Box-Behnken design

Run order	Coded Levels			Yield of Cellulose (%)	
	A (%)	B (°C)	C (min)	Experimental	Predicted
1	2	100	180	64.19	64.27
2	5	75	120	67.10	67.06
3	3.5	75	180	72.83	72.85
4	3.5	75	180	72.81	72.85
5	2	50	180	56.61	56.67
6	5	50	180	70.87	70.81
7	3.5	100	240	59.45	59.40
8	3.5	75	180	72.89	72.84
9	3.5	50	120	69.73	69.78
10	3.5	75	180	72.86	72.81
11	2	75	120	59.25	59.20
12	5	100	180	56.43	56.50
13	2	75	240	56.82	56.87
14	3.5	75	180	72.79	72.85
15	3.5	50	240	70.07	70.02
16	3.5	100	120	73.54	73.59
17	5	75	240	55.40	55.45

Thermogravimetric Analysis (TGA)

The thermal behavior of raw and isolated cellulose from *ensete ventricosum* pseudo stem fiber was performed on a thermal analyzer (HTC_1, Ethiopia) to determine the thermal stability of the samples under a nitrogen atmosphere in a platinum crucible for about 60 min with a flow rate of 25 mL/min. The heating cycle used is a constant heating rate of 20 °C/min from room temperature to 700 °C (Dube, 2022).

Fourier-transformed Infrared (FTIR) Spectra Analysis

Infrared spectroscopy was used to examine the chemical functional groups and structural differences between raw ensete fiber and cellulose. A thermos-scientific (iS50 ABX, Addis Ababa Science and Technology University, Ethiopia) spectrometer was used to gather Fourier transfer infrared (FTIR) spectra with a resolution of 16 cm^{-1} in the 4,000–400 cm^{-1} range. To make pastilles, each sample was first ground into a powder and combined with KBr (Dube, 2022; Pires et al., 2013).

X-ray Diffraction (XRD) Analysis

An X-ray diffraction (XRD) examination was used to look into the crystallinity index (%CrI) of raw fiber and cellulose samples. The X-ray diffraction patterns of several powder samples were obtained for this investigation using a diffractometer (XRD-7000 X-RAY DIFFRACTOMETER, Shimadzu Corporation, Japan) that was scanned at room temperature between 2θ with a diffraction angle in the range of 10° to 80° and a step size of 0.02°. The applied current was 30 mA while the accelerating voltage was 40 kV.

$$CrI = \frac{I200 - Iam}{I200} \quad (1)$$

$$CrI = \left(\frac{I200 - Iam}{I200}\right) \times 1000 \quad (2)$$

Where Iam is the minimum intensity of the amorphous region alone at peak 2θ = 18°, and I200 is the maximum intensity of the peak at 2θ = 22.65°, which corresponds to both the crystalline and amorphous regions.

Scanning Electron Microscopy (SEM) Analysis

Scanning electron microscopy JCM, 6000 plus (Addis Ababa Science and Technology University, Ethiopia) was used to investigate the surface morphology of samples of raw ensete and cellulose at a working distance of 500–10 µm and with an accelerating voltage of 15 kV. Prior to observation, all samples were covered with gold (Dube, 2022).

Results And Discussions

Model Selection and Regression Analysis

Table 2, Table 3, Table 4, and Table 5 present the sequential model sum of squares, model summary statistics, and analysis of variance for the quadratic model, respectively.

Table 2
Analyses of several models using the sum of squares

Source	Sum of square	DF	Mean square	F-value	P-value	Remark
Mean Vs total	74,288.5	1	74, 288.5			
Linear Vs mean	141.12	3	47.04	0.912	0.462	
2F1 Vs linear	192.72	3	64.24	1.34	0.315	
Quadratic Vs 2F1	**477.93**	**3**	**159.31**	**42,767.9**	**< 0.0001**	**suggested**
Cubic Vs quadratic	0.02	3	0.0064	3.63	0.122	Aliased
Residual	0.007	4	0.002			
Total	75,100.3	17	4417.7			

The experimental data were analyzed using design-expert software to generate a regression equation, equation, which represented the cellulose yield versus the function of the independent variables. Accordingly, only the quadratic model's p value is 0.0001 in the sum of squares analysis (Table 2), indicating that the model is significant. According to variance analysis, the quadratic model's F value is 2421 (Table 4) and its lack of fit mean square value is 0.007 (Table 4), all of which show that it is appropriate for the experimental design. The ratio of the explained variation to the overall variation, which measures the model's fitness, is generally known as the coefficient of determination R^2. A high R^2 value implies that the dependent variables in the model are relevant. The quadratic model's R^2 value is 0.998 (Table 3), which shows how well it can account for the system's actual behavior.

Table 3
Summaries of the model's statistics

Source	Std. deviation	R2	Adjusted R2	Predicted R2	Press	Remark
Linear	7.18	0.174	-0.017	-0.46	1184.6	
2F1	6.91	0.411	0.06	-0.902	1543.8	
Quadratic	**0.061**	**0.998**	**0.999**	**0.999**	**0.32**	**Suggested**
Cubic	0.042	0.999	1.00		+	Aliased

The experimental data were analyzed in Design-expert 11 to generate a regression equation that described the cellulose yield as a function of the independent variables, as shown in Eq. (2):

$$CelluloseYield = 72.85 + 1.61A - 1.7B - 3.49C - 5.46AB - 2.32AC - 3.61BC - 9.68A^2 - 1.13B^2 - 3.52C^2 \ldots\ldots\ldots\ldots\ldots\ldots$$

Where the coded variables for the concentration of sodium hydroxide, the reaction temperature, and the reaction time are A, B, and C, respectively.

Table 4
ANOVA for response surface quadratic model

Source	Sum of square	DF	Mean square	F-Value	P-Value	Remark
Model	811.77	9	90.20	2421	0.0001	Significant
Residual	0.03	7	0.004			
Lack of fit	0.02	3	0.007	3.6	0.1224	Not Significant
Pure Error	0.007	4	0.002			
Core Total	811.80	16				

Table 5
Summary of independent variables coefficients and standard deviation

Factors	Coefficient	DF	Standard error	95% CI low	95% CI high
Intercept	72.85	1	0.03	72.79	72.91
A: [NaOH]	1.65	1	0.022	1.56	1.66
B: Temperature	-1.70	1	0.022	-1.76	-1.65
C: Time	-3.49	1	0.022	-3.54	-3.44
AB	-5.46	1	0.031	-5.53	-5.39
AC	-2.32	1	0.031	-2.39	-25
BC	-3.61	1	0.031	-3.68	-3.54
A^2	-9.70	1	0.03	-9.75	-9.61
B^2	-1.13	1	0.03	-1.2	-1.06
C^2	-3.52	1	0.03	-3.6	-3.45

The Analysis of Variables Interaction Effect and Optimization

Response surface plots, in general, display the interaction effects of two factors on the response of interest while maintaining the level of other variables (i.e., zero). Elliptical plots show a substantial interaction between the variables, while circular contour plots show an insignificant interaction between the variables.

Figure 2 depicts the impact of reaction temperature, sodium hydroxide, and their interaction on cellulose yield. The breakdown of non-cellulose components and the improvement of cellulose yield are both significantly influenced by sodium hydroxide concentration. The alkali treatment of ensete fiber could not produce a larger yield of cellulose at a lower sodium hydroxide concentration. The output of cellulose rises as the concentration reaches a specific point. The best yield may be attained at a sodium hydroxide concentration of (2.6 to 4.4%) and a reaction temperature of 65 to 100°C. Overreaction is the cause of the decreased cellulose yield at increasing sodium hydroxide concentrations. Cellulose was broken down into its component sugar molecules when an over-reaction with an excess of sodium hydroxide concentration and a higher reaction temperature took place.

The impact of reaction time and sodium hydroxide concentration on cellulose yield is depicted in Fig. 3. Reaction time is crucial in the breakdown of non-cellulose materials. The reaction of the fiber could not take place efficiently in a short amount of time. The yield of cellulose rises as response time reaches a particular point. At 150–190 minutes of reaction time and a sodium hydroxide concentration of 2.2–3.9%, the best yield is obtained. The overreaction is the cause of the decline in cellulose yield with increasing reaction times. Cellulose was split into its constituent sugar molecules when the over-reaction took place with too much reaction time.

Figure 4 illustrates how reaction temperature and time affect cellulose production. The breakdown of ensete fiber into its constituent parts, such as cellulose, depends significantly on reaction time. The ensete fiber could not be properly treated with alkali in a short amount of time. The yield of cellulose increases when the reaction time rises to a particular point. The best yield may be attained at reaction temperatures between 65 and 100 ℃ and reaction times between 150 and 190 min. The overreaction is the cause of the decreased cellulose yield with longer reaction times. Cellulose was disintegrated into its constituent parts when the over-reaction took place with too much reaction time.

The best conditions are 73 ℃ for the reaction temperature; 157 min for the reaction duration; and 3.8% sodium hydroxide concentration, according to the computer program's forecast (Fig. 5). In these circumstances, the yield of cellulose from ensete fiber reaches 73.9%, which is not substantially different from the projected value of 72.91% at a 95% confidence interval (Table 5).

Thermogravimetric Analysis

Figure 6 displays the TGA and DTG curves of cellulose and ensete fiber (a) (b). As the figure revealed, the weight loss during the thermal deterioration of samples occurs at three different temperatures. The initial thermal degradation of ensete fiber results in a small weight loss at 192.5 ℃, which is followed by a large weight loss between 192.5 and 327.5 ℃, and finally a moderate weight loss up to 485 ℃. There is a noticeable weight decrease for cellulose between 247.5 and 352.5 ℃. Additionally, according to the DTG curves, the maximal weight loss for ensete fiber and cellulose peaks at 350 and 355 ℃, respectively. When compared with cotton the TGA patterns of *ensete ventricosum* pseudo stem fiber cellulose is different because of its low cellulose (77.74 and 86.67 for raw and treated fiber, respectively) content and high lignin (6.68 and 1.01 for raw and treated fiber, respectively) content (Dube, 2022). All of the aforementioned findings show that cellulose has greater thermal stability than raw ensete fiber. This is because raw ensete fiber contains more non-cellulosic components than cellulosic components, which encourages heat degradation of the samples (Dube, 2022; Normand et al., 2014).

Fourier-transformed Infrared (FTIR) Spectra Analysis

Figure 7 displays the FTIR spectra of raw ensete fiber and cellulose. The presence of a stretching vibration of the O-H group, which is related to the intramolecular hydrogen bond of cellulose, results in the characteristic bands of 3277.00-3348 cm^{-1} and 2922.7 cm^{-1} associated with stretching vibration C-H. The figure clearly demonstrates how, when the fiber is subjected to chemical treatment, the transmittance for this region gradually changes. The transmittance showed an increments and the peak becomes sharper due to alkali treatment and an increase in cellulose content (Dube, 2022; Kallel et al.,

2016; Merci et al., 2015). Lower absorbance intensity ratios are found in the absorption band at 1,634.7 cm^{-1}, which is associated with the vibration of carbonyl groups and adsorbed water molecules. The opening of the terminal glycopyranose rings or the oxidation of the C-OH groups may be the cause of the occurrence of this peak (Hemmati et al., 2018). In ensete fiber, 1327.74 cm^{-1} corresponds to the CH2 scissoring of cellulose, hemicellulose, and lignin as well as the stretching of the C-O ring of syringyl lignin and the condensed G ring of lignin (Teli & Terega, 2017). The peak at 1315.45cm^{-1} is associated with the rocking vibration of CH2 in the cellulose alcohol group (Prado & Spinacé, 2019). The peak at 1002 cm^{-1} illustrates the C-O-C pyranose vibrating stretching ring of cellulose (Rahman et al., 2017).

X-ray Diffraction (XRD) Analysis

The X-ray diffraction (XRD) patterns of cellulose and ensete fiber are displayed in Fig. 8. In accordance with the distinctive diffraction peaks of cellulose I, XRD patterns exhibit diffraction peaks at 2θ = 15.2, 17.4, 22.2, and 34.8, which correspond to the (1–10), (110), (002), and (004) crystallographic planes (Chandra CS et al., 2016). *At those diffraction angles, sharp peaks are clearly seen, which represent cellulose I type indicating higher crystallinity of microfibers. As clearly observed from the figure, the crystallinity of the sample increases with stepwise chemical pretreatments (*Rosa et al., 2010). *And it also may be caused by the aluminum sample holder that was used in this study.* Ensete fiber and cellulose have a crystallinity index of 44.1 and 62.3 percent, respectively. The decrease and elimination of cellulose's non-cellulosic components and disordered regions are responsible for the observed rise in the crystallinity index of cellulose (Hemmati et al., 2018). Additionally, the crystal lattice in the (002) plane appears to be more perfect than that of an ensete fiber, as seen by the diffraction peak of 22.2 becoming shaper.

Scanning Electron Microscopy (SEM) Analysis

Figure 9a&b, respectively, display SEM images of cellulose and ensete fiber. SEM micrographs show that the morphologies of raw ensete fiber and separated cellulose are clearly distinct from one another. Raw fiber image (Fig. 9, a) reveals a smoother surface, which was a result that was anticipated given the presence of extractives such as wax and pectin (Galiwango et al., 2019; Kathirselvam et al., 2019; Normand et al., 2014). In contrast to raw fiber, processed Ensete fiber had a rough surface with fragments of fiber bundles and an irregular form and size. The primary cause of this is the destruction of non-cellulose components of the fiber by chemical pretreatments, which results in the removal of the protective layer of alpha cellulose (Galiwango et al., 2019).

Conclusions

The extraction of cellulose from ensete fiber a plentiful, affordable, and easily accessible material was successful. In the current work, the effects of mechanical treatment, chemical pretreatment (alkali and bleaching), and its alkali treatment condition on the yield and properties of cellulose have been investigated. These effects affect the functional groups, chemical composition, morphology, thermal properties, and crystallinity of ensete fiber. An extraordinarily high amount of cellulose was produced by the effective and gradual removal of the lignin layer and hemicellulose from the biomass, which makes it easier to extract CNCs afterwards. The amount of cellulose and the reaction conditions have a significant impact on the yield of cellulose. So attaining a good CNC yield and the right characteristics requires correct reaction conditions for chemical pretreatment of cellulose. The outcomes for various characterizations show that ensete fiber is a productive, enduring, and regenerative source for the isolation of cellulose nanocrystals. The optimal sodium hydroxide concentration, reaction temperature, and reaction time were found to be 3.8%, 73°C, and 157 minutes after optimizing the alkali treatment conditions for cellulose isolation. The substantial potential of the ensete ventricosum pseudo stem fiber for the extraction of cellulose nanocrystals is revealed by the high crystallinity index and good thermal stability of the obtained cellulose.

Declarations

Statements and Declarations

Authors’ Contributions

Abnet Mengesha Dube carried out the experiment, collected the data, assessed the data, developed the text, and authored the final manuscript. Bulcha Jifara and Melkiyas Dirba participated in editing and proofreading of all steps, including the manuscript.

With best regards,

Abnet Mengesha Dube

Ethical Approval and Consent of Participate

The research work is the original work of the authors except for the citation which have been duly acknowledged. With the submission of this manuscript, we would like to undertake that the above-mentioned manuscript was not previously submitted to Journal of Cellulose or elsewhere.

Consent for Publication

All authors mutually agreed that it should be submitted to the Journal of Cellulose.

Availability of Data and Materials

The data and materials used in this study are available on request from the corresponding author.

Funding

The authors affirm that they did not accept any money, grants, or other forms of support for the creation of this publication.

Competing Interests

The author states that the work reported in this article was not impacted by any known conflicting financial interests or personal connections.

Authors' Information

Title	Full name	Degree	Department	Institute	Email	Area of interest	Authors' order
Mr.	Abnet Mengesha Dube	MSc	Chemical Engineering	Wolkite University	abnetm817@gmail.com	Bio-waste Valorization, Bioenergy, CNCs	First
Mr.	Bulcha Jifara Daba	MSc	Chemical Engineering	Haromaya University	bulchajifara64@gmail.com	Bio-waste Valorization, Bioenergy, Energy	Co
Mr.	Melkiyas Dirba Muleta	MSc	Chemical Engineering	Haromaya University	melkidm10@gmail.com	Bio-waste Valorization, Bioenergy, Energy	Co

References

1. Abdul Khalil, H. P. S., Issam, A. M., Ahmad Shakri, M. T., Suriani, R., & Awang, A. Y. (2007). Conventional agro-composites from chemically modified fibres. Industrial Crops and Products, *26*(3), 315–323. https://doi.org/10.1016/j.indcrop.2007.03.010
2. ASPINALL, G. O. (1980). Chemistry of Cell Wall Polysaccharides. In *Carbohydrates: Structure and Function* (Vol. 3). ACADEMIC PRESS, INC. https://doi.org/10.1016/b978-0-12-675403-2.50018-1
3. Berhanu, H., Kiflie, Z., Miranda, I., Lourenço, A., Ferreira, J., Feleke, S., Yimam, A., & Pereira, H. (2018). Characterization of crop residues from false banana /ensete ventricosum/ in Ethiopia in view of a full-resource valorization. PLoS ONE, *13*(7). https://doi.org/10.1371/journal.pone.0199422
4. Bosha, T., Lambert, C., Riedel, S., Gola, U., Melesse, A., & Biesalski, H. K. (2019). Validation of the CIMI-ethiopia program and seasonal variation in maternal nutrient intake in enset (False banana) growing areas of Southern Ethiopia. International Journal of Environmental Research and Public Health, *16*(16), 1–13. https://doi.org/10.3390/ijerph16162852
5. Chandra CS, J., George, N., & Narayanankutty, S. K. (2016). Isolation and characterization of cellulose nanofibrils from arecanut husk fibre. Carbohydrate Polymers, *142*, 158–166. https://doi.org/10.1016/j.carbpol.2016.01.015
6. Cheesman, W., Megersa, H. G., & Lemma, D. T. (2022). Integrated Pest Management System of Enset (Ensete ventricosum (Welw.) Cheesman) in Ethiopia:A Review. Journal of Natural Sciences Research, *April*. https://doi.org/10.7176/jnsr/13-9-03
7. Davison, B. H., Parks, J., Davis, M. F., & Donohoe, B. S. (2013). Plant Cell Walls: Basics of Structure, Chemistry, Accessibility and the Influence on Conversion. *Aqueous Pretreatment of Plant Biomass for Biological and Chemical Conversion to Fuels and Chemicals*, 23–38. https://doi.org/10.1002/9780470975831.ch3
8. Dube, A. M. (2022). Isolation and characterization of cellulose nanocrystals from Ensete ventricosum pseudo-stem fiber using acid hydrolysis. Biomass Conversion and Biorefinery. https://doi.org/10.1007/s13399-022-02987-z
9. Dufresne, A. (2019). Nanocellulose Processing Properties and Potential Applications. Current Forestry Reports. https://doi.org/10.1007/s40725-019-00088-1
10. Fekadu, D., & Ledin, I. (1997). *Weight and chemical composition of the plant parts of enset and the intake and degradability of enset by cattle*. *49*, 249–257.
11. Flauzino Neto, W. P., Silvério, H. A., Dantas, N. O., & Pasquini, D. (2013). Extraction and characterization of cellulose nanocrystals from agro-industrial residue - Soy hulls. Industrial Crops and Products, *42*(1), 480–488. https://doi.org/10.1016/j.indcrop.2012.06.041
12. Gabriel, T., Belete, A., Syrowatka, F., Neubert, R. H. H., & Gebre-Mariam, T. (2020). Extraction and characterization of celluloses from various plant byproducts. International Journal of Biological Macromolecules, *158*, 1248–1258. https://doi.org/10.1016/j.ijbiomac.2020.04.264
13. Galiwango, E., Abdel Rahman, N. S., Al-Marzouqi, A. H., Abu-Omar, M. M., & Khaleel, A. A. (2019). Isolation and characterization of cellulose and α-cellulose from date palm biomass waste. Heliyon, *5*(12), e02937. https://doi.org/10.1016/j.heliyon.2019.e02937
14. Gong, J., Li, J., & Xu, J. (2017). cellulose sources with various polymorphs. RSC Advances, *7*, 33486–33493. https://doi.org/10.1039/C7RA06222B
15. Habibi, Y., Lucia, L. A., & Rojas, O. J. (2010). Cellulose nanocrystals: Chemistry, self-assembly, and applications. Chemical Reviews, *110*(6), 3479–3500. https://doi.org/10.1021/cr900339w

16. Hemmati, F., Jafari, S. M., Kashaninejad, M., & Barani Motlagh, M. (2018). Synthesis and characterization of cellulose nanocrystals derived from walnut shell agricultural residues. International Journal of Biological Macromolecules, *120*, 1216–1224. https://doi.org/10.1016/j.ijbiomac.2018.09.012
17. Henrique, M. A., Silvério, H. A., Flauzino Neto, W. P., & Pasquini, D. (2013). Valorization of an agro-industrial waste, mango seed, by the extraction and characterization of its cellulose nanocrystals. Journal of Environmental Management, *121*, 202–209. https://doi.org/10.1016/j.jenvman.2013.02.054
18. Kallel, F., Bettaieb, F., Khiari, R., García, A., Bras, J., & Chaabouni, S. E. (2016). Isolation and structural characterization of cellulose nanocrystals extracted from garlic straw residues. Industrial Crops and Products, *87*, 287–296. https://doi.org/10.1016/j.indcrop.2016.04.060
19. Kathirselvam, M., Kumaravel, A., Arthanarieswaran, V. P., & Saravanakumar, S. S. (2019). International Journal of Biological Macromolecules Isolation and characterization of cellulose fi bers from Thespesia populnea barks: A study on physicochemical and structural properties. International Journal of Biological Macromolecules, *129*, 396–406. https://doi.org/10.1016/j.ijbiomac.2019.02.044
20. Klemm, D., Cranston, E. D., Fischer, D., Gama, M., Kedzior, S. A., Kralisch, D., Kramer, F., Kondo, T., Lindström, T., Nietzsche, S., Petzold-Welcke, K., & Rauchfuß, F. (2018). Nanocellulose as a natural source for groundbreaking applications in materials science: Today's state. Materials Today, *21*(7), 720–748. https://doi.org/10.1016/j.mattod.2018.02.001
21. Lin, Q., Huang, Y., & Yu, W. (2021). Effects of extraction methods on morphology, structure and properties of bamboo cellulose. Industrial Crops and Products, *169*(May), 113640. https://doi.org/10.1016/j.indcrop.2021.113640
22. Merci, A., Urbano, A., Victória, M., Grossmann, E., & Tischer, C. A. (2015). Properties of microcrystalline cellulose extracted from soybean hulls by reactive extrusion. FRIN, *73*, 38–43. https://doi.org/10.1016/j.foodres.2015.03.020
23. Miao, Q., Chen, L., Huang, L., Tian, C., Zheng, L., & Ni, Y. (2014). A process for enhancing the accessibility and reactivity of hardwood kraft-based dissolving pulp for viscose rayon production by cellulase treatment. Bioresource Technology, *154*, 109–113. https://doi.org/10.1016/j.biortech.2013.12.040
24. Mohammed, B., Gabel, M., & Karlsson, L. M. (2013). *Nutritive values of the drought tolerant food and fodder crop enset*. *8*(20), 2326–2333. https://doi.org/10.5897/AJAR12.1296
25. Mtibe, A., Linganiso, L. Z., Mathew, A. P., Oksman, K., John, M. J., & Anandjiwala, R. D. (2015). A comparative study on properties of micro and nanopapers produced from cellulose and cellulose nanofibres. Carbohydrate Polymers, *118*, 1–8. https://doi.org/10.1016/j.carbpol.2014.10.007
26. Normand, M. Le, Moriana, R., & Ek, M. (2014). Isolation and characterization of cellulose nanocrystals from spruce bark in a biorefinery perspective. Carbohydrate Polymers, *111*, 979–987. https://doi.org/10.1016/j.carbpol.2014.04.092
27. Nurfeta, A., Eik, L. O., Tolera, A., & Sundstøl, F. (2008). *Chemical composition and in sacco dry matter degradability of different morphological fractions of 10 enset (Ensete ventricosum) varieties*. *146*, 55–73. https://doi.org/10.1016/j.anifeedsci.2007.12.003
28. Nurfeta, A., Tolera, A., Eik, L. O., & Sundstøl, F. (2008). The supplementary value of different parts of enset (Ensete ventricosum) to sheep fed wheat straw and Desmodium intortum hay. Livestock Science, *119*(1–3), 22–30. https://doi.org/10.1016/j.livsci.2008.02.010
29. Olango, T. M., Tesfaye, B., Catellani, M., & Pè, M. E. (2014a). Indigenous knowledge, use and on-farm management of enset (Ensete ventricosum (Welw.) Cheesman) diversity in Wolaita, Southern Ethiopia. Journal of Ethnobiology and Ethnomedicine, *10*(1), 1–18. https://doi.org/10.1186/1746-4269-10-41
30. Olango, T. M., Tesfaye, B., Catellani, M., & Pè, M. E. (2014b). *Indigenous knowledge, use and on-farm management of enset (Ensete ventricosum (Welw .) Cheesman) diversity in Wolaita, Southern Ethiopia*. 1–18.
31. Owolabi, F. A. T., Deepu, A. G., Thomas, S., Shima, J., Rizal, S., Sri Aprilia, N. A., & Abdul Khalil, H. P. S. (2020). Green Composites From Sustainable Cellulose Nanofibrils. In *Encyclopedia of Renewable and Sustainable Materials*. https://doi.org/10.1016/b978-0-12-803581-8.11422-5
32. Pires, W., Neto, F., Alves, H., Oliveira, N., & Pasquini, D. (2013). Extraction and characterization of cellulose nanocrystals from agro-industrial residue – Soy hulls. Industrial Crops & Products, *42*, 480–488. https://doi.org/10.1016/j.indcrop.2012.06.041
33. Prado, K. S., & Spinacé, M. A. S. (2019). Isolation and characterization of cellulose nanocrystals from pineapple crown waste and their potential uses. International Journal of Biological Macromolecules, *122*, 410–416. https://doi.org/10.1016/j.ijbiomac.2018.10.187
34. Rahman, N. H. A., Chieng, B. W., Ibrahim, N. A., & Rahman, N. A. (2017). Extraction and characterization of cellulose nanocrystals from tea leaf waste fibers. Polymers, *9*(11), 1–11. https://doi.org/10.3390/polym9110588
35. Rojas, O. J. (2016). Cellulose Chemistry and Properties: Fibers, Nanocelluloses and Advanced Materials. In *Advances in Polymer Science 271* (Vol. 271). http://www.springer.com/series/12%0Ahttp://link.springer.com/10.1007/978-3-319-26015-0
36. Rosa, M. F., Medeiros, E. S., Malmonge, J. A., Gregorski, K. S., Wood, D. F., Mattoso, L. H. C., Glenn, G., Orts, W. J., & Imam, S. H. (2010). Cellulose nanowhiskers from coconut husk fibers: Effect of preparation conditions on their thermal and morphological behavior. Carbohydrate Polymers, *81*(1), 83–92. https://doi.org/10.1016/j.carbpol.2010.01.059
37. Seid, N., Griesheimer, P., & Neumann, A. (2022). Investigating the Processing Potential of Ethiopian Agricultural Residue Enset/Ensete ventricosum for Biobutanol Production. Bioengineering, *9*(4). https://doi.org/10.3390/bioengineering9040133
38. Southon, J. R., & Magana, A. L. (2010). A comparison of cellulose extraction and aba pretreatment methods for ams 14C dating of ancient wood. Radiocarbon, *52*(3), 1371–1379. https://doi.org/10.1017/S0033822200046452
39. Teli, M. D., & Terega, J. M. (2017). Chemical, Physical and Thermal Characterization of Ensete ventricosum Plant Fibre. International Research Journal of Engineering and Technology, *04*(12).
40. Tsegaye, A., & Struik, P. C. (2021). Enset (Ensete ventricosum (Welw.) Cheesman) kocho yield under different crop establishment methods as compared to yields of other carbohydrate-rich food crops. NJAS - Wageningen Journal of Life Sciences, *49*(1), 81–94. https://doi.org/10.1016/S1573-5214(01)80017-8

41. Xing, L., Gu, J., Zhang, W., Tu, D., & Hu, C. (2018). Cellulose I and II nanocrystals produced by sulfuric acid hydrolysis of Tetra pak cellulose I. Carbohydrate Polymers, *192*(February), 184–192. https://doi.org/10.1016/j.carbpol.2018.03.042
42. Yemata, G. (2020). Ensete ventricosum: A Multipurpose Crop against Hunger in Ethiopia. *Scientific World Journal*, *2020*. https://doi.org/10.1155/2020/6431849
43. Yemataw, Z., Bekele, A., Blomme, G., Muzemil, S., Tesfaye, K., & Jacobsen, K. (2018). A review of enset [Ensete ventricosum (Welw.) Cheesman] diversity and its use in Ethiopia. Fruits, *73*(6), 301–309. https://doi.org/10.17660/th2018/73.6.1
44. Zerihun Yemataw, Henoke Fikre, Sadik Muzemil, J. B. and T. M. (2021). *Annotated Bibilography of Enset (Ensete ventricosum (Welw.) Cheesman) in Getinet Alemaw, Agdew Bekele and Fekadu Gurmu (Editors)*. *May*, 92.
45. Zhang, X., Wang, F., & Keer, L. M. (2015). Influence of surface modification on the microstructure and thermo-mechanical properties of bamboo fibers. Materials, *8*(10), 6597–6608. https://doi.org/10.3390/ma8105327

Figures

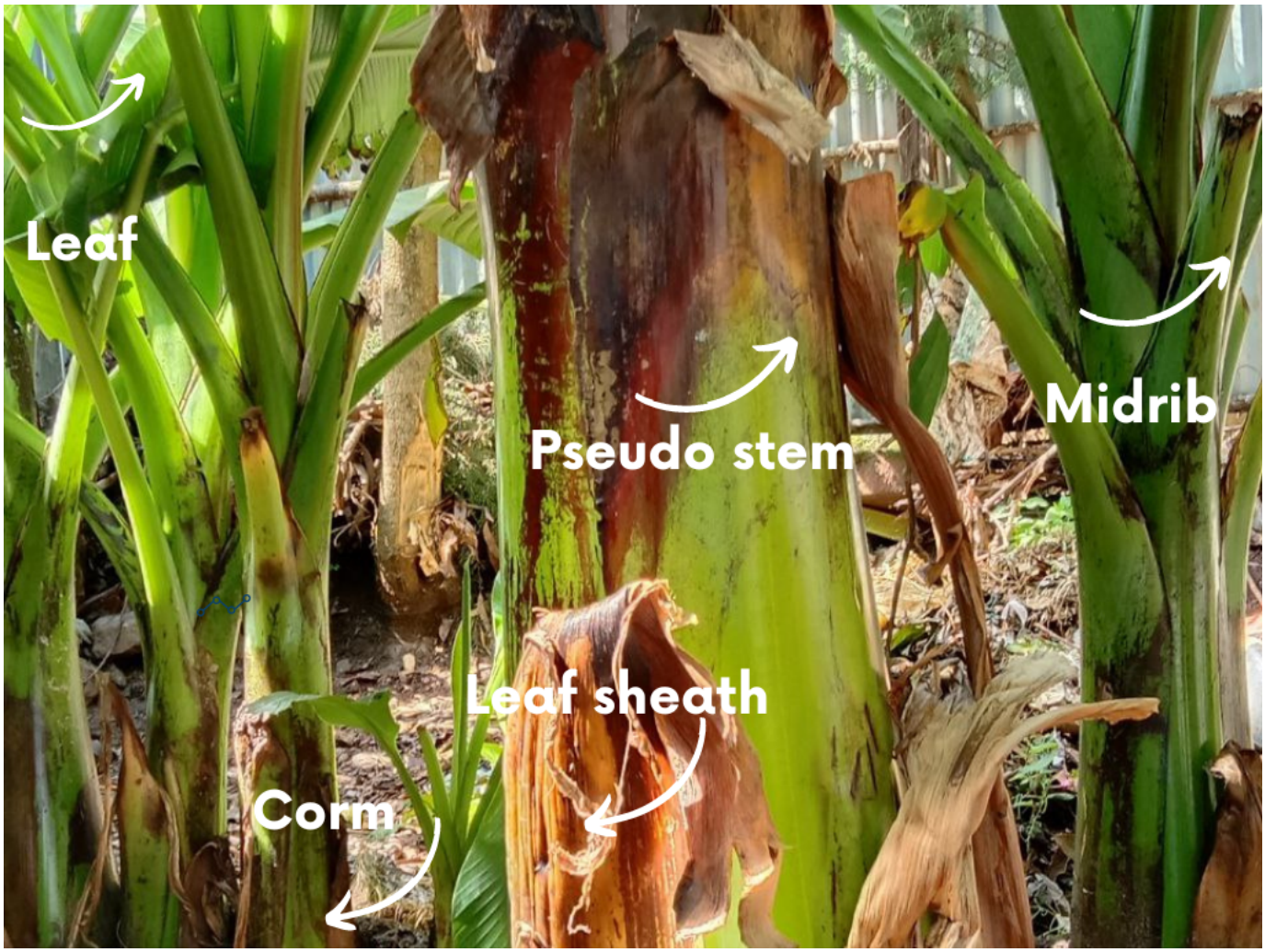

Figure 1

Ensete ventricosum's parts (I took this picture on a personal ensete farm in Gubre, Ethiopia.

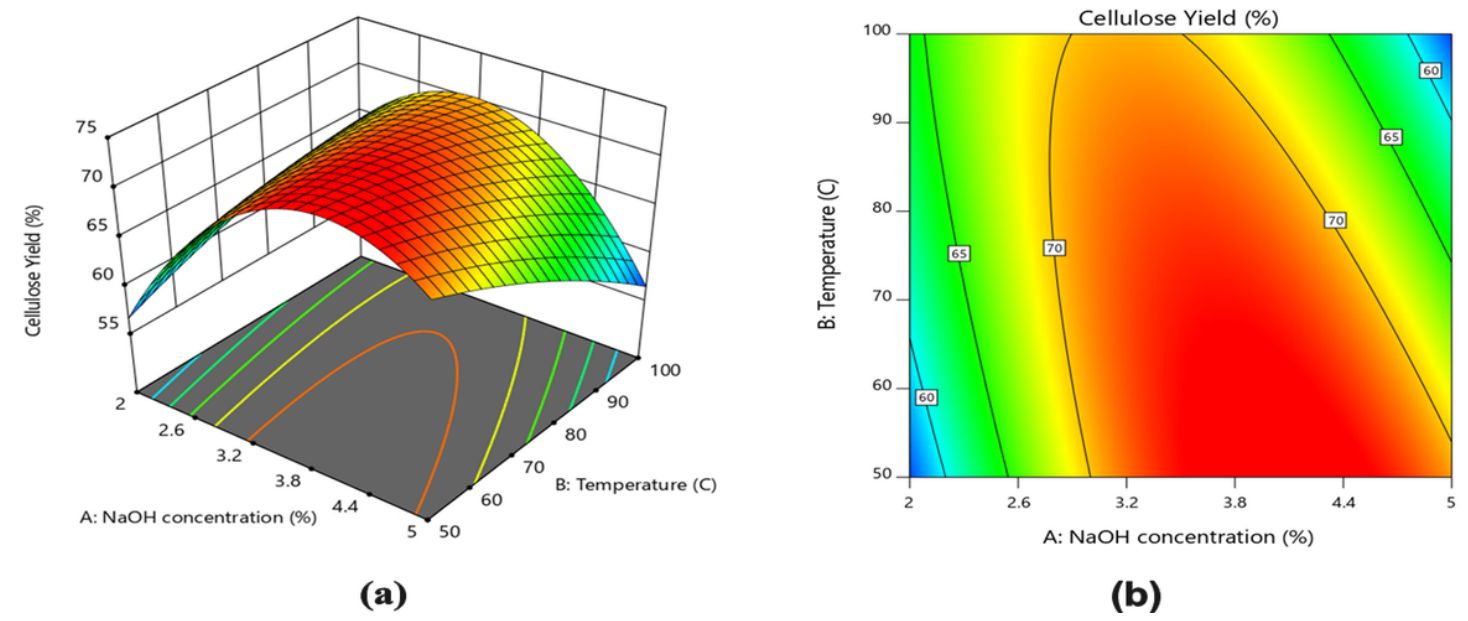

Figure 2

Response surface (a) and contours (b) depicting the effect of reaction temperature and NaOH concentration on the yield of cellulose

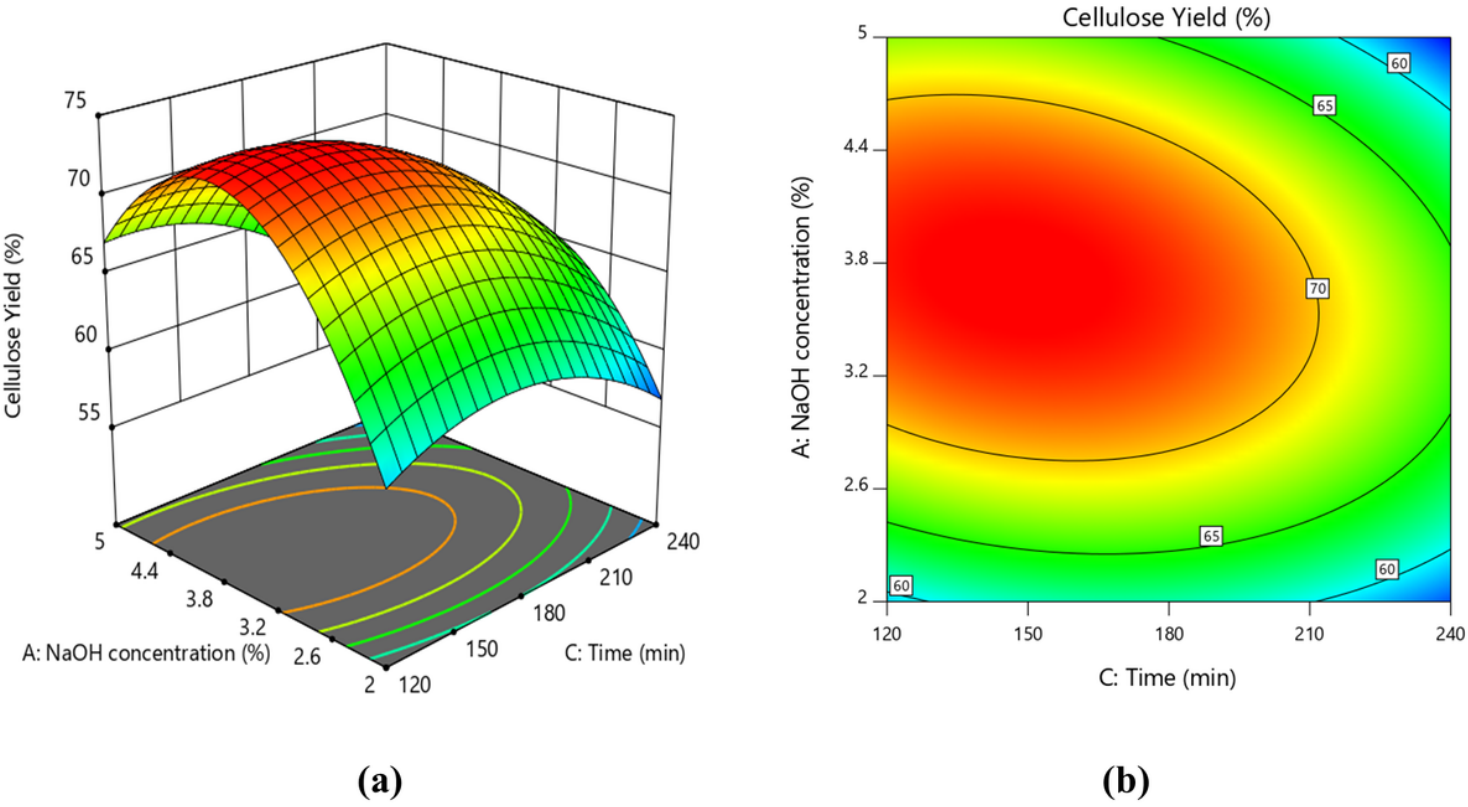

Figure 3

Response surface (a) and contours (b) depicting the effect of NaOH concentration and reaction time on the yield of cellulose

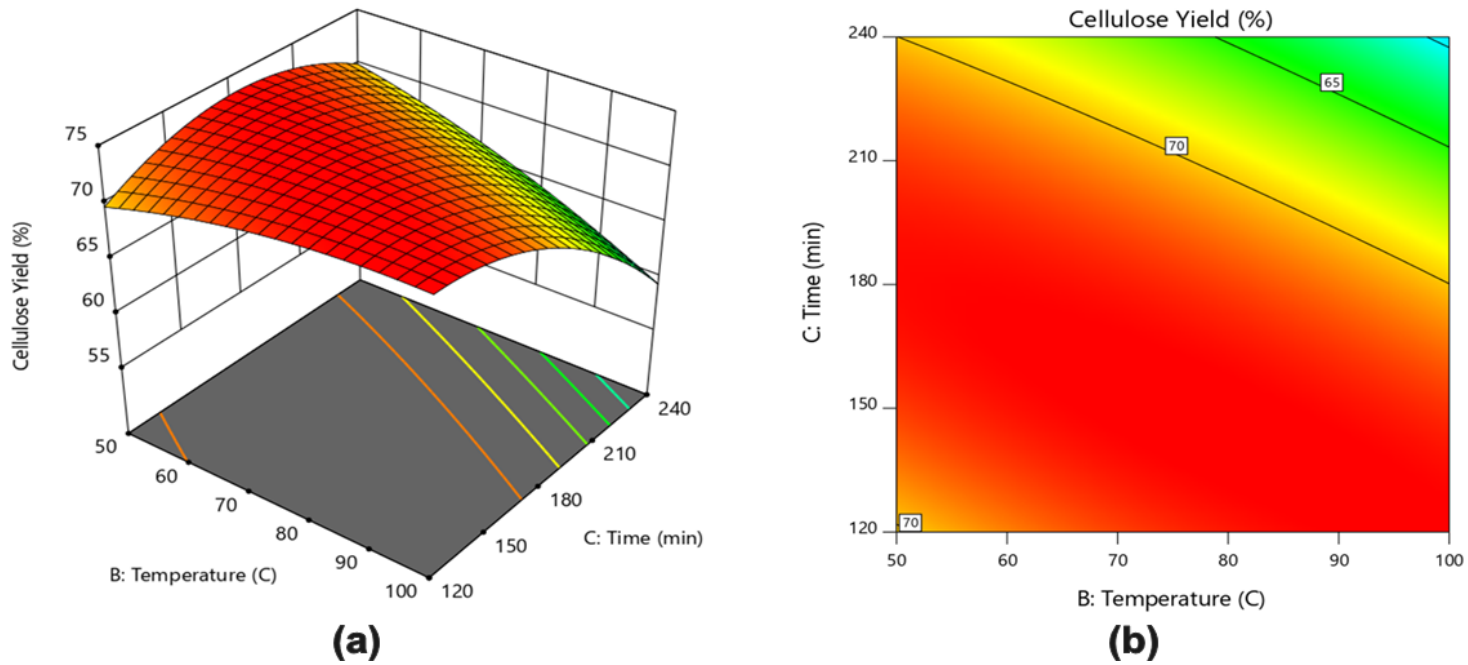

Figure 4

Response surface (a) and contours (b) depicting the effect of reaction temperature and reaction time on the yield of cellulose

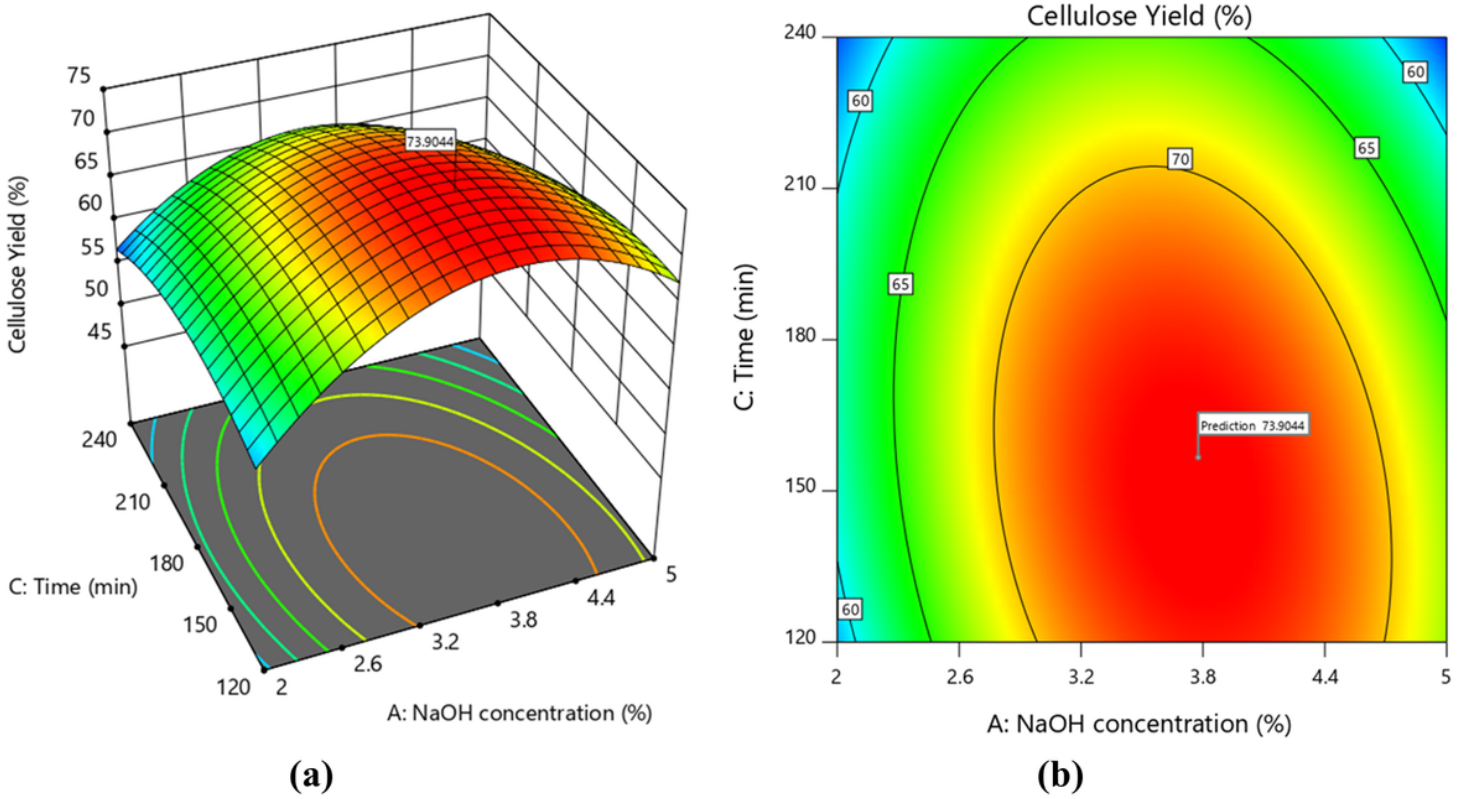

Figure 5

Response surface (a) and contours (b) of the optimized yield of cellulose

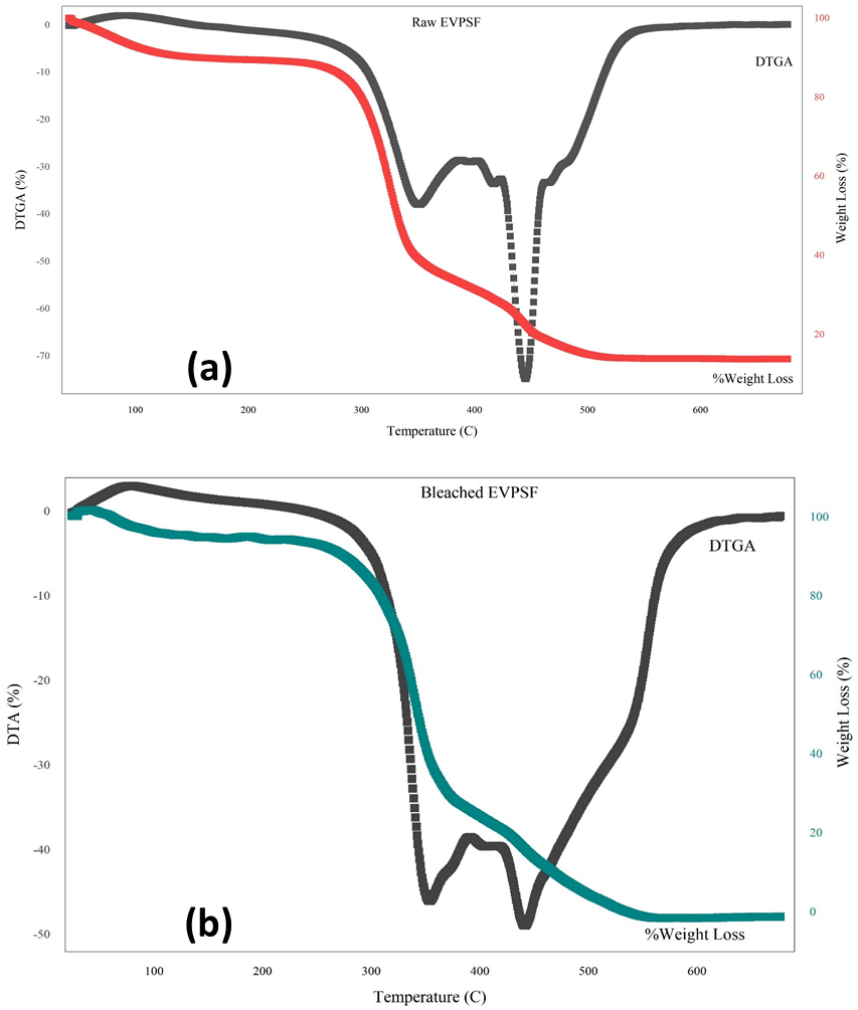

Figure 6

TG-curves and DTG-curves of raw fiber (a) and cellulose (b)

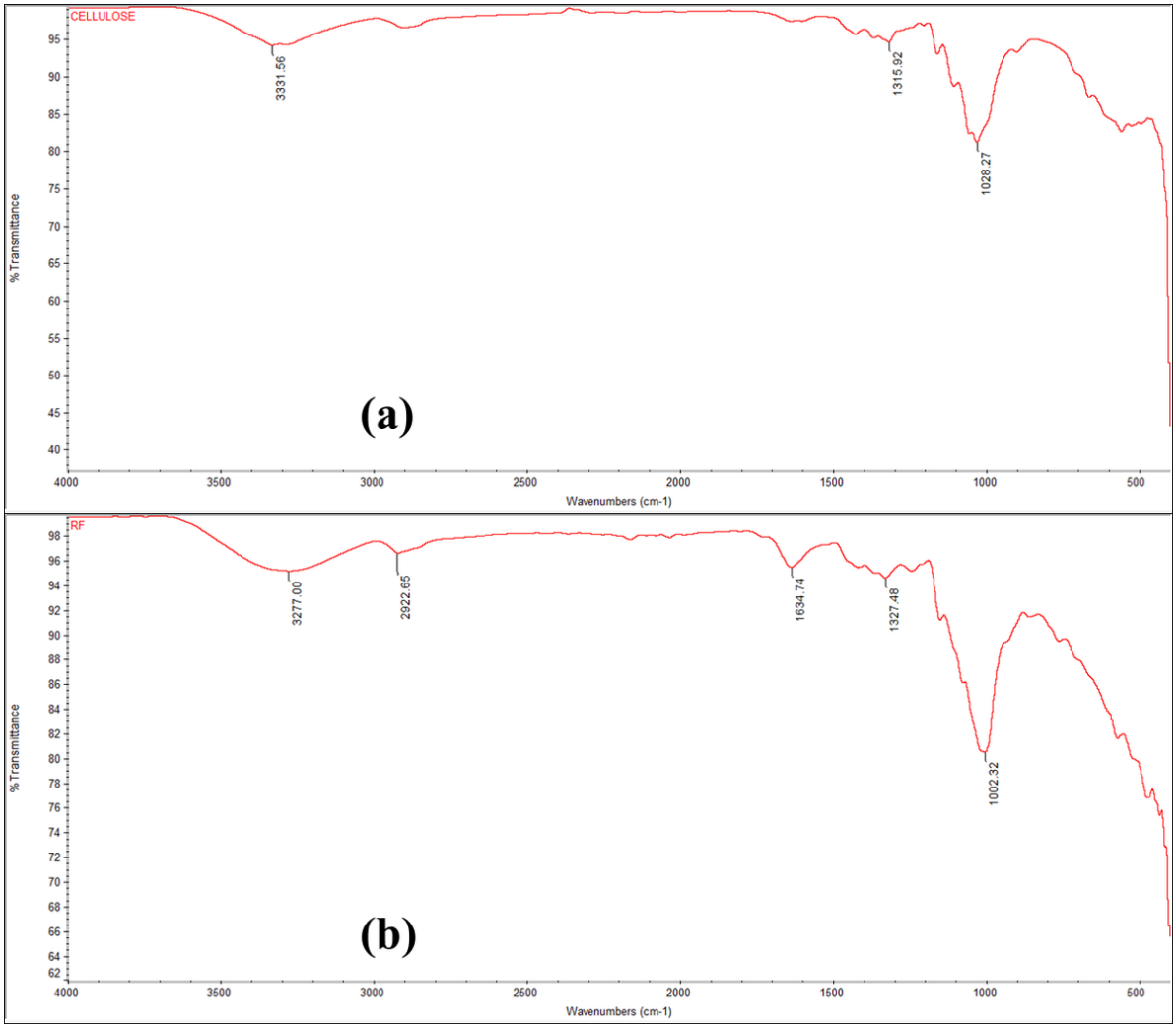

Figure 7

FTIR spectra of isolated cellulose (a) and raw ensete fiber (b)

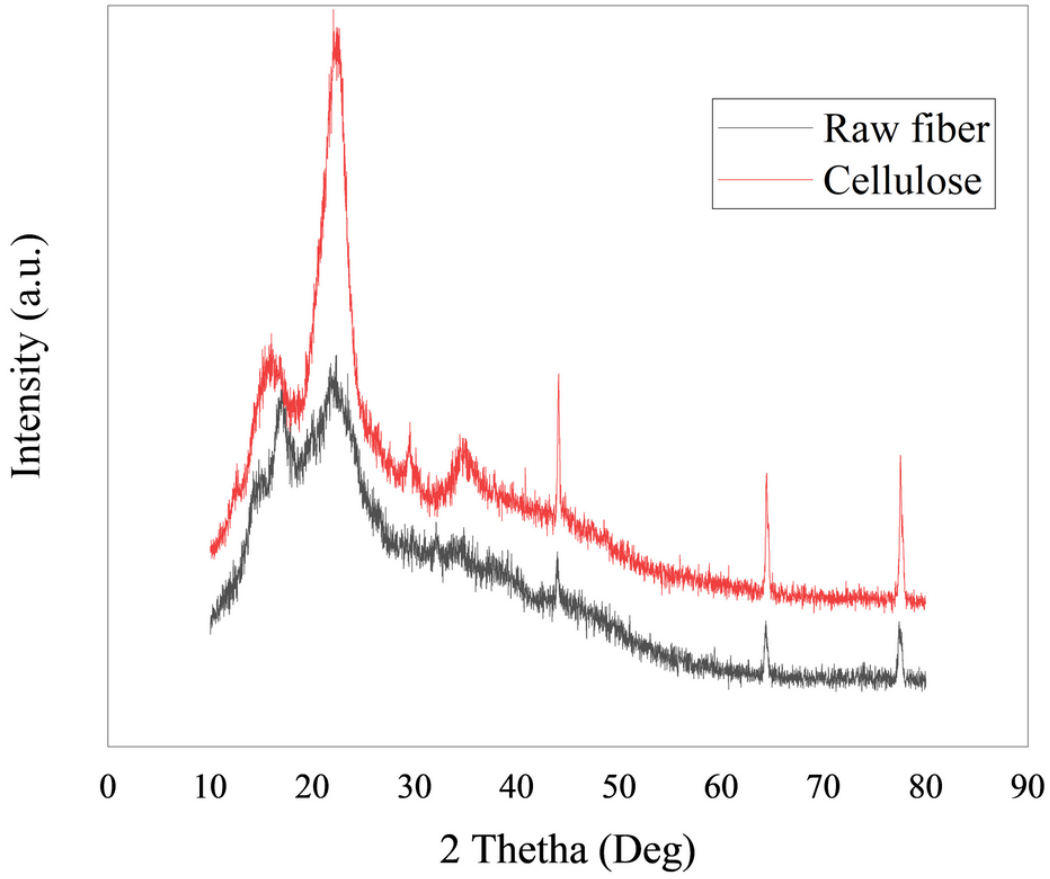

Figure 8

Raw fiber and cellulose XRD patterns

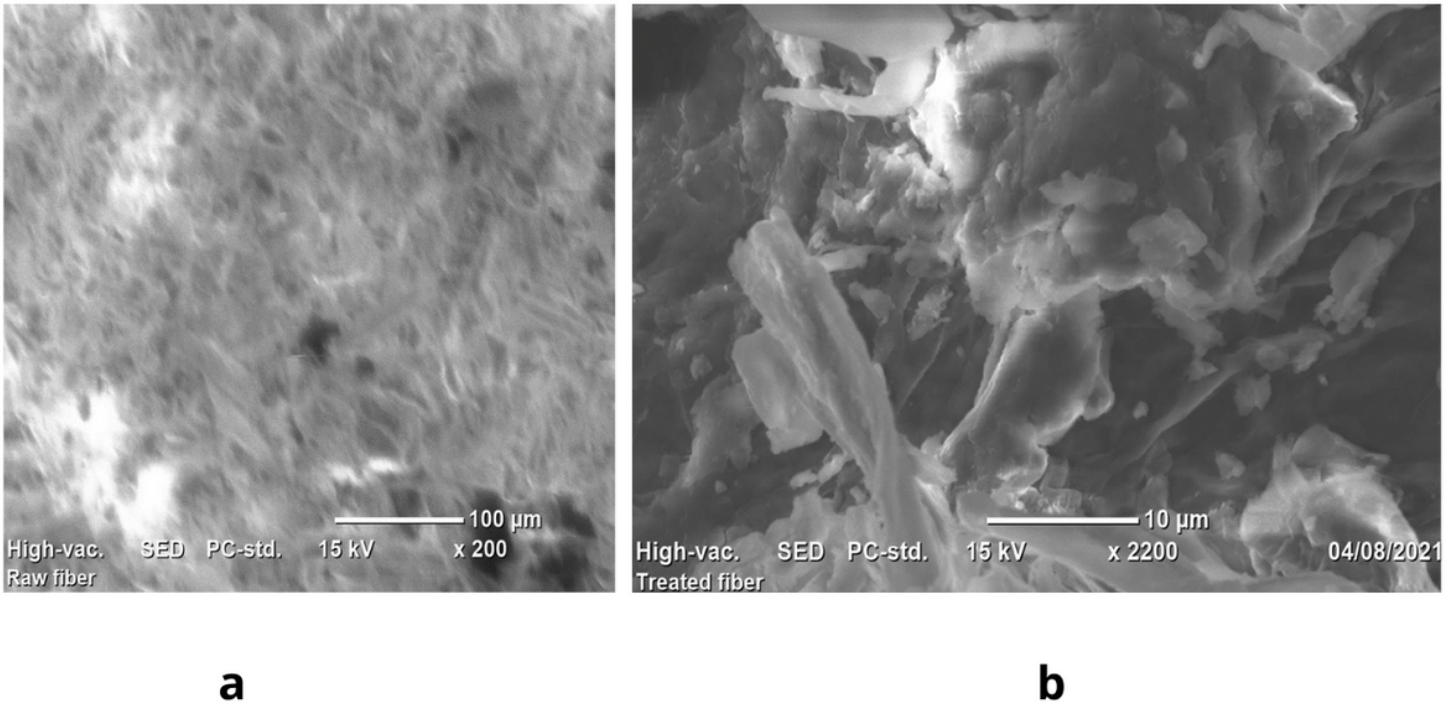

Figure 9

SEM images of raw fiber (a) and cellulose (b)